Er^{3+}-doped SiO_2-TeO_2-ZnO-Na_2O thin film fabricated by ultrafast laser plasma doping under different ambient atmospheres

S. A. Kamil[a,b,*], G. Jose[c]
[a]*Faculty of Applied Sciences, Universiti Teknologi MARA, 40450 Shah Alam, Selangor, Malaysia*
[b]*NANO-SciTech Laboratory, Centre for Functional Materials and Nanotechnology, Institute of Science, Universiti Teknologi MARA, 40450 Shah Alam, Selangor Malaysia*
[c]*School of Chemical and Process Engineering, University of Leeds, Clarendon Road, Leeds LS2 9JT, UK*

Er^{3+}-ions doped SiO_2-ZnO-Na_2O thin films were fabricated using ultrafast laser plasma doping (ULPD) techniques under different ambient atmospheres; vacuum, nitrogen, oxygen and argon gas. The thickness of the layer produced depends on the ambient atmosphere during fabrication. The layer fabricated under a vacuum is the thinnest among all of the samples. In addition, the surface layer for the sample fabricated under a vacuum environment seems to be relatively smoother compared with those of the others. XRD patterns show that all samples are in a mixed amorphous-crystalline phase. All the Raman spectra exhibited a similar pattern, except for the intensity of the Si peak which depended on the thickness of the obtained layer. The PL intensity for each sample corresponds to the amount of Er^{3+} ions embedded in the doped layer. However, all samples still exhibited silicate-based characteristics, indicating nitrogen in Si_3N_4 was lost in the form of nitrogen gas during fabrication.

(Received October 11, 2023; Accepted January 2, 2024)

Keywords: Ultrafast lasers, Laser ablation, Optical materials, Er^{3+} doped glasses, Thin film

1. Introduction

Over the past few years, the ultrafast laser has been used to dope rare earth ions into the Si_3N_4-on-silicon [1,2], fused silica [3,4] and silica-on-silicon [5,6] substrate. Ultrafast laser plasma doping is one of the doping techniques that can be employed to dope optically active ions into the substrate. This technique is a recent approach for producing a thin film for optical applications. The high-intensity laser pulse is employed to ionise, melt and evaporate the surface of the target material. This causes the explosive removal of material which can also be called ablation and induce plasma formation. The plasma then expands in a perpendicular direction at the rate of a few km/s [4] to the heated substrate and strikes the surface. The interfacial reaction between the target plasma and substrate surface, with the aid of thermal diffusion, forms a modified layer consisting of a combination of the target material and the surface substrate. The thickness (nm to μm) and quality of the modified layer vary depending on the process parameter and type of target material and substrate used. Although the mechanism in ULPD mimics the PLD technique, but some of the process involved has their own novelty and speciality that cannot be found in samples produced by the PLD technique.

The choice of laser pulse duration is the main parameter influencing the laser ablation process. For ULPD, a femtosecond laser (fs-laser) is used to ablate the target material. The fundamental of this process is light-matter interaction at very short time scales and involves some complicated processes. When the fs-laser bombards the target material, the photon energy will be absorbed by atoms in the target material and later transferred the energy to the electron. The absorbed energy promotes an electron to be excited from its ground state to its excited state. The excitation

* Corresponding author: suraya_ak@uitm.edu.my
https://doi.org/10.15251/CL.2024.211.11

mechanism is different for metal, semiconductor and insulator. Generally, for an fs-laser, it has a high intensity which is in the range of 10^{12}-10^{19} W/cm^2 [7] and this leads to strong non-linear absorption. For an insulator like glass, an electron in the valence band is excited to the conduction band by non-linear photoionization, specifically by multi-photon ionisation and/or tunnelling ionisation.

Several important parameters are involved in the ULPD process. Among them are substrate temperature, repetition rate, laser energy, ambient atmosphere and background gas pressure. The optimum substrate temperature is very crucial in order to produce a quality doped layers [2]. Higher laser energy and repetition rate offer a thicker doped layer while higher background gas pressure can reduce the doped layer thickness [5,6]. Meanwhile, ULPD permits the doping process to occur under vacuum, inert or reactive background gas environment. The existence of background gas in a chamber plays a significant role in ULPD as it affects the properties of the fabricated layer. The mean free path and kinetic energy of the ablated nanoparticles and ions can be modified by the presence of background gas pressure as it can attenuate, scatter and thermalize the energy of the ion in the plasma plume in the chamber. Therefore, it is very important to choose the type of background gas because each background gas can react with the plasma plume in a different way. To the best of our knowledge, the influence of different ambient atmospheres in ULPD using Si_3N_4 substrate has still not been reported. In this study, we report the effect of different ambient atmospheres in ULPD on structural, morphological and optical properties of Er^{3+}-doped SiO_2-TeO_2-ZnO-Na_2O thin film.

2. Materials and methods

2.1. Preparation of the target glass

Glass with compositions of 79.5TeO_2–10ZnO-10Na_2O-0.5Er_2O_3 denoted as Er-TZN was fabricated using a conventional melt-quenching technique. All the raw materials (TeO_2, ZnO, Na_2O and Er_2O_3) used to synthesize Er-TZN glass are analytical grade chemicals of purity > 99.99%. In brief, all the chemicals were mixed and ground into a fine powder using a marble pestle and mortar after they were weight out according to their specific molar masses. The mixture was then placed into a gold crucible and left to be melted in the furnace with a low oxygen flow rate for 3 hours at 875 °C. The melted mixture was then quickly poured into a preheated brass mould and annealed at 295 °C for 4 hours to eliminate mechanical strains and residual thermal. Then, the mixture was cooled down to room temperature at 0.5 °C/min. The obtained glass was polished using a polishing machine (Buehler, Motopol, 2000) with various grades of silicon carbide paper (Buehler Grit P1200, P2400, and P4000) until the glass surface is flat and smooth.

2.2 Laser ablation

A commercial Coherent Ti: Sapphire LIBRA laser with pulse duration 100 fs, wavelength centred at 800 nm and pulse repetition rate of 1 kHz was used to ablate the Er-TZN. The fs-laser beam was focused on to the target glass surface through a transparent window of the vacuum chamber at an angle of incidence 60°. The target's surface needed to be polished before being placed into the target holder in order to obtain a flat surface that helps control the plasma plume direction which can affect the uniformity of the film produced. The target was then rotated and rasterize according to a set programme. This was to ensure that the laser could ablate the target surface uniformly. The Si_3N_4-on-silicon substrate with Si_3N_4 thickness of 1 μm was then placed opposite the focal spot above the target at a distance of 70 mm. The substrate was then heated at 650°C with a programmable heating element at a rate up to 50 °C per minute. The ablations process was performed in a vacuum chamber for four hours under different ambient atmospheres. The process parameters used to prepare all of these samples are tabulated in Table 1. The sample that was fabricated in a vacuum is labelled SV while SO, SN and SA represent oxygen, nitrogen and argon environments, respectively.

Table 1. The parameters used to dope Er-TZN into Si_3N_4-on-silicon substrate under different ambient atmospheres.

Process parameters	Operating conditions
Substrate	Si_3N_4 (t=1 μm)-on-silicon
Target material	$79.5TeO_2$-10ZnO-$10Na_2O$-$0.5Er_2O_3$ (Er-TZN)
Fs-laser energy	80 μJ
Fs-laser repetition rate	1.0 kHz
Substrate temperature	650 °C
Ablation period	4 hours
Background gas pressure (Sample name)	Vacuum – 6 x 10^{-5} Torr (SV), 70 mTorr O_2 (SO), 70 mTorr N_2 (SN) and 70 mTorr Ar (SA)

2.3 Sample characterization

A scanning electron microscope (Hitachi SU8230) was employed to determine the cross-section morphology and thickness for all the samples, prepared with different ambient atmospheres. Elemental mapping was obtained by using the energy dispersive X-ray (EDS, Oxford Instruments PLC, Oxford, UK). The image surface of the thin films was captured using bench-top scanning electron microscopy (Hitachi TM3030Plus). The crystallinity of the thin films was characterized using X-ray diffraction (XRD) (Philips X'Pert). The measurement of photoluminescence (PL) spectra and corresponding PL lifetime were undertaken by a PL spectrometer (Edinburgh Instruments FLS920 series). Renishaw inVia micro was used to determine Raman spectra of the samples and the measurement were done using the 514 nm excitation wavelength with a power of 25 mW at room temperature.

3. Results and discussion

The micrographs obtained, Figure 1 (a)-(d), show the doped layer on Si_3N_4-on silicon with different background atmospheres whilst the thickness of each doped layer together with the Si_3N_4 layer underneath it, is presented in Table 2. The original Si_3N_4 layer thickness is decreased due to the alteration of Si_3N_4 surface by the transformation into a doped layer (Figure 1 (a)-(d)). Figure 2 exhibited the EDS element mapping of the doped layer for SV sample. This result can be ascribed that the target material managed to penetrate into Si_3N_4 layer, modified the orginal Si_3N_4 network and formed a doped layer that consist the mixture of Er-TZN and Si_3N_4. However, the obtained doped layers were not smooth and uniform. Although elements from the target glass managed to enter Si_3N_4, a homogeneous layer failed to be obtained due to a high melting temperature (1900 °C) and rigid structure of Si_3N_4.

It can be seen that the doped layer under vacuum (SV) is the thinnest among all of the samples. The thinner doped layer recorded for the SV is believed to be related to the plume dynamics during the process. In such high vacuum conditions, when the laser ablates the target, the generated plume leaves the target with very high energy towards the substrate surface. The bombardment of these very energetic particles/ions onto the substrate/doped layer surface induces these particles to be re-sputtered or reflected when they bombard the substrate of the already formed film [8,9].

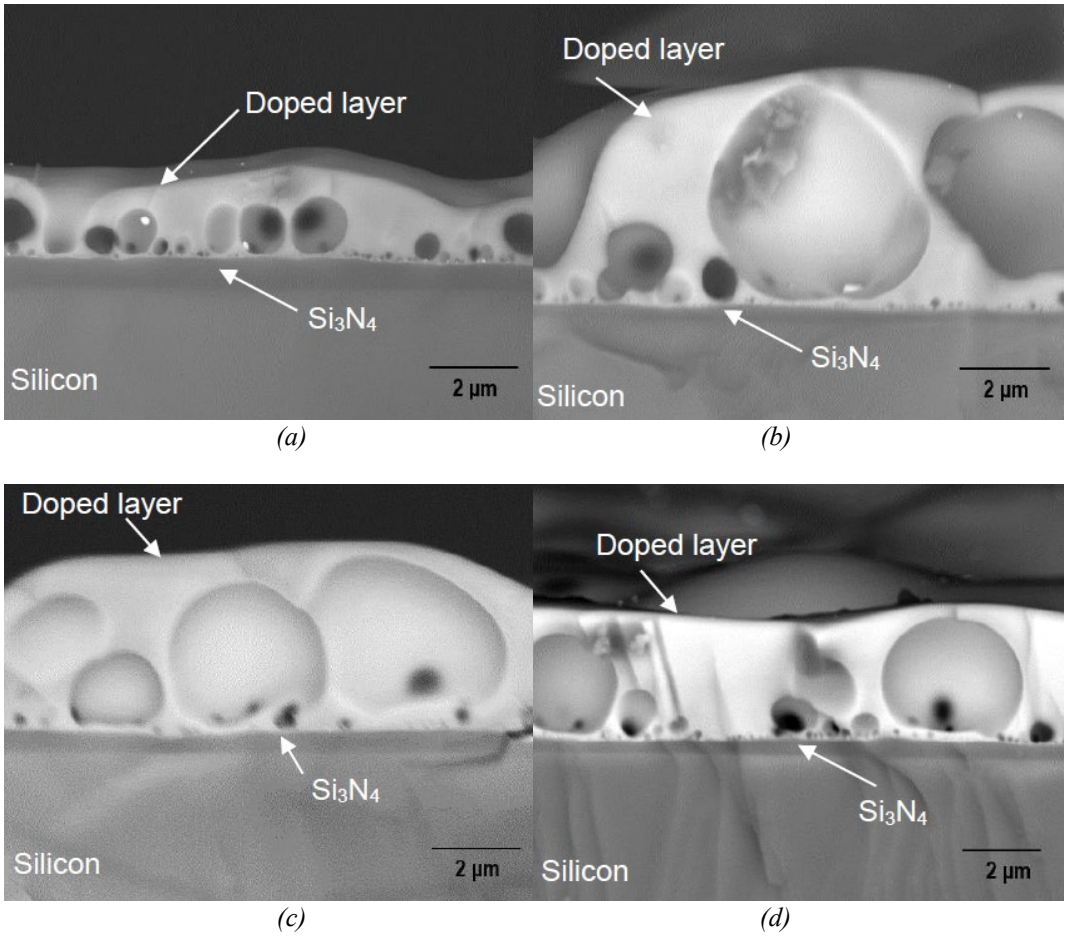

Fig. 1. Backscattered cross-section SEM image of samples doped with Er-TZN under (a) vacuum (SV) and a background gas of (b) oxygen (SO), (c) nitrogen (SN), and (d) argon (SA).

Table 2. Thickness of upper layer and Si_3N_4 underneath measured by SEM for samples SV, SO, SN and SA.

Sample	**Thickness (µm)**	
	Upper layer	**Si_3N_4 under the upper layer**
SV	2.1 ± 0.2	0.62 ± 0.04
SO	5.4 ± 0.4	0.34 ± 0.04
SN	4.5 ± 0.3	0.35 ± 0.05
SA	3.0 ± 0.2	0.40 ± 0.06

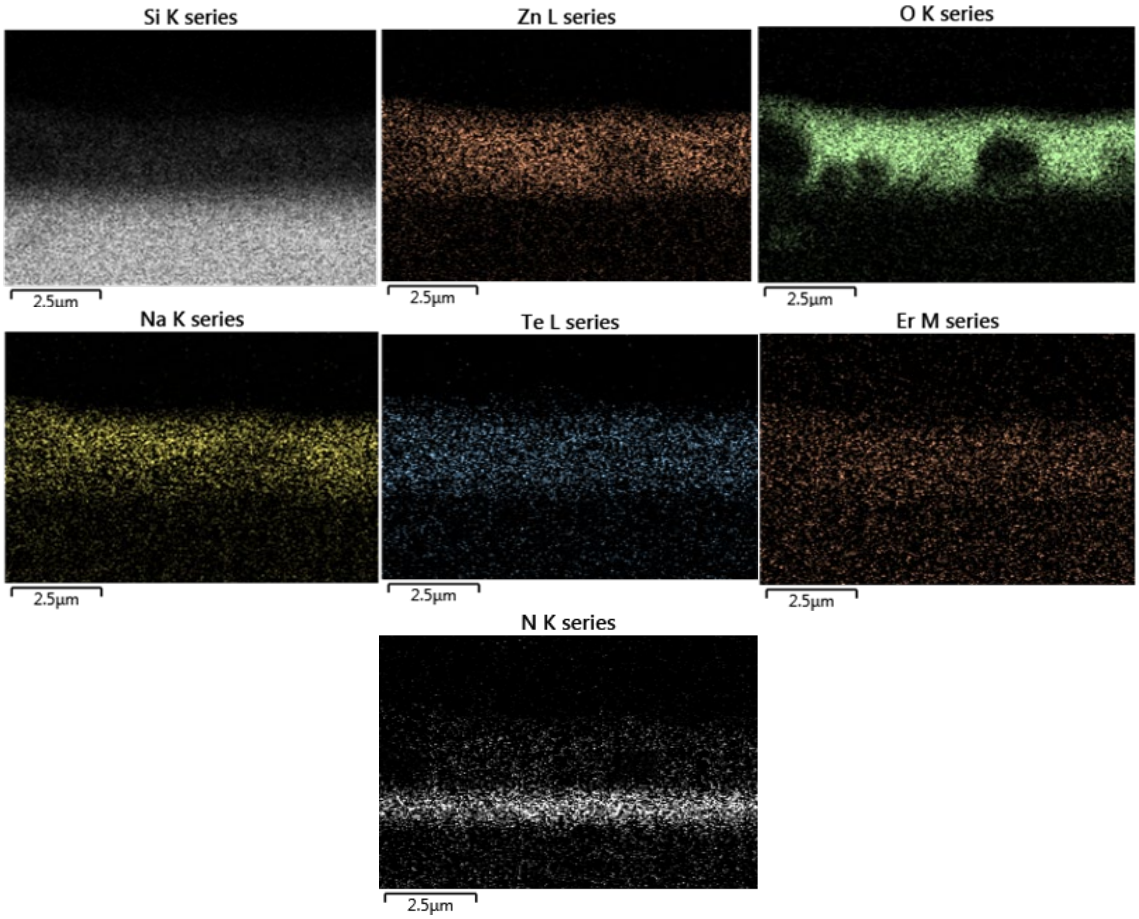

Fig. 2. EDS element mapping for sample SV.

The very high kinetic energy of a particle in the plasma plume can be reduced by deliberately introducing a background gas in the chamber at low pressures. The presence of the background gas creates collision events which occur between the ablated particle and background gas that will scatter the plumes from their initial trajectories [10,11] and increase the residence time of particles in the plume. This gives ample time for the particles to nucleate, agglomerate and enlarge their sizes prior to reaching the substrate [12]. As a consequence, they will be less mobile on the substrate surface [11].

Since the argon atom is bigger than the nitrogen and oxygen atoms, the probability of a collision incident between particles in the plume with Ar atoms is higher, resulting in a shorter mean free path and bigger particle size. Therefore, a thinner layer is produced than for the samples fabricated under O_2 or N_2 atmospheres. The mean free path can be estimated by using equation 1 [12,13]:

$$\lambda_m = \frac{k_B T}{\sqrt{2}\pi x^2 P} \quad (1)$$

where k_B is the Boltzmann constant, T is the temperature of the gas, x is the collisional cross-section and P is the gas pressure. The mean paths for the Ar and O_2 environments are estimated to be around 1.767 x 10^{-7} m and 2.475 x 10^{-7} m respectively, and it is predicted to be higher under vacuum conditions [12]. For the N_2 atmosphere, it is expected that the mean free path is quite similar to that of O_2 because both have almost similar mass density. However, it appears that the thickness of the doped layer for sample SO is higher than that of SN although SN is fabricated with a lighter background gas. This is probably because O_2 is more reactive than N_2 and chemical reactions between O_2 and particles within the plume may have occurred. It is anticipated that the reaction between O_2 from the background gas with the ablated particles will form single monoxide or

multioxide molecules. This heavier monoxide or multioxide molecules experience less scattering to the flank side compared to lighter elements [14]. This might be the cause of the doped layer for the SO samples being thicker than that for the SN samples.

The surfaces of the doped layers for the samples prepared under various environmental conditions were recorded by SEM and shown in Figure 3 (a)-(d). Figure 3 (a) displays a surface image sample prepared in a high vacuum environment while those prepared under oxygen, nitrogen and argon atmospheres are presented in Figure 3 (b) – (d). Among the images, the surface layer for SV seems to be relatively smoother. This was probably due to the particles that travelled to the substrate directly from the target (without or with very few collisions), and this resulted in the sizes of the particles which impinged on the substrate being smaller. The size of a bump on the surface increases when heavier gas is used. In addition, a heavier gas increases the residence time of the particles in the plume which makes the particle become bigger, the collisions between the background gas and the particles in the plume become more severe, leading to an increased broadening of the plume angular distribution. For a heavy background gas, the broadening is more critical than for a light gas. Light species in the plume tend to be much more scattered than heavy species, and this leads to the appearance of large particles on the film [8]. This phenomenon led to the formation of large particles for SA samples.

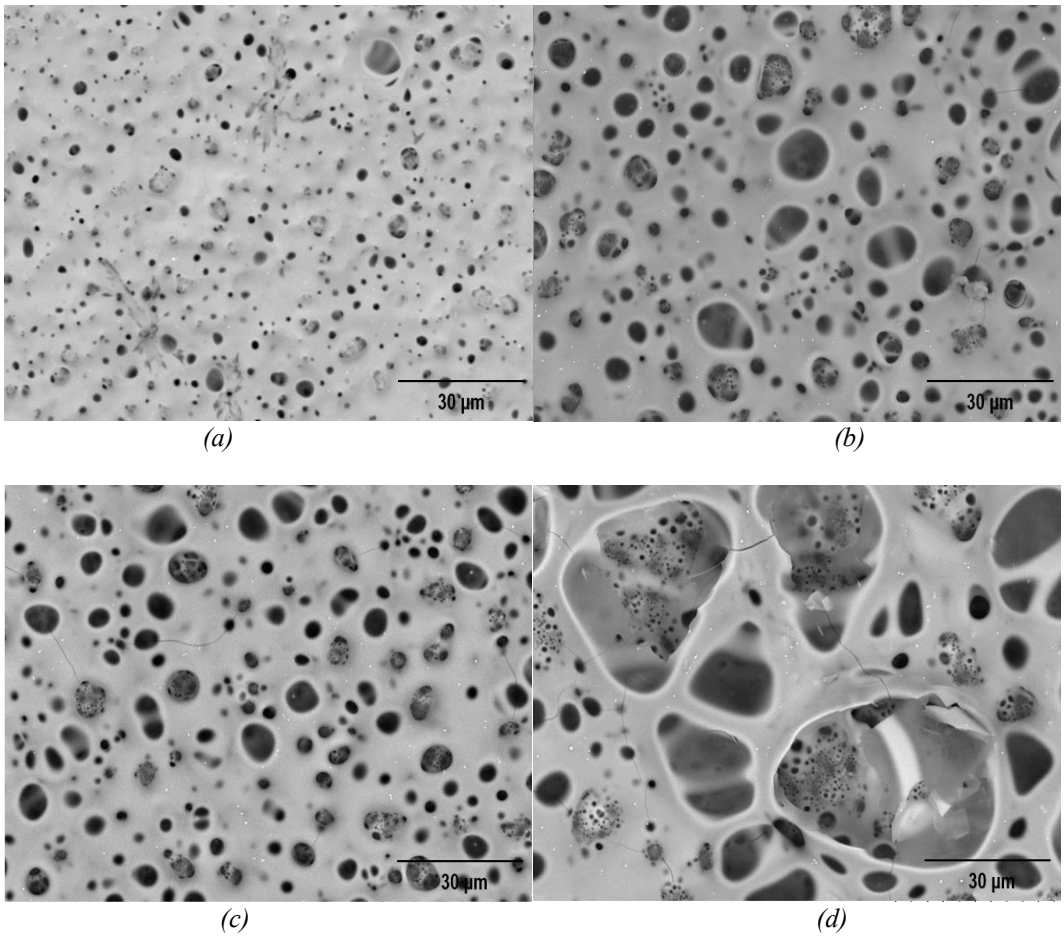

Fig. 3. SEM micrograph for the surface of doped layers prepared under (a) vacuum (SV), (b) oxygen (SO), (c) nitrogen (SN) and argon (SA).

Figure 4 (a)-(d) shows the XRD patterns of the doped layers on Si_3N_4-on-silicon fabricated in different atmospheres. The patterns show that all samples are is in a mixed amorphous-crystalline phase. The indexed peaks assigned to the possible crystalline structures are also shown in Figure 4

(a)-(d). The sample prepared in an oxygen environment clearly exhibited a higher intensity of crystalline peak, which indicated a greater degree of crystallinity [15]. This is probably attributable to the interaction of oxygen gas with species in the plume. The energy exchange and heat generation associated with the oxidation process expedited the crystallisation of the doped layer and improved the crystallinity [16]. On the other hand, the longer residence stays time for plume particles in the argon atmosphere could also have enhanced the building of a more stable crystal bridge [17] and subsequently, therefore, increased the crystalline phase (Figure 4 (d)). Furthermore, the high interaction of ablated species with the argon atoms eventually increased the plasma plume temperature, which also helped to increase the crystallisation [18].

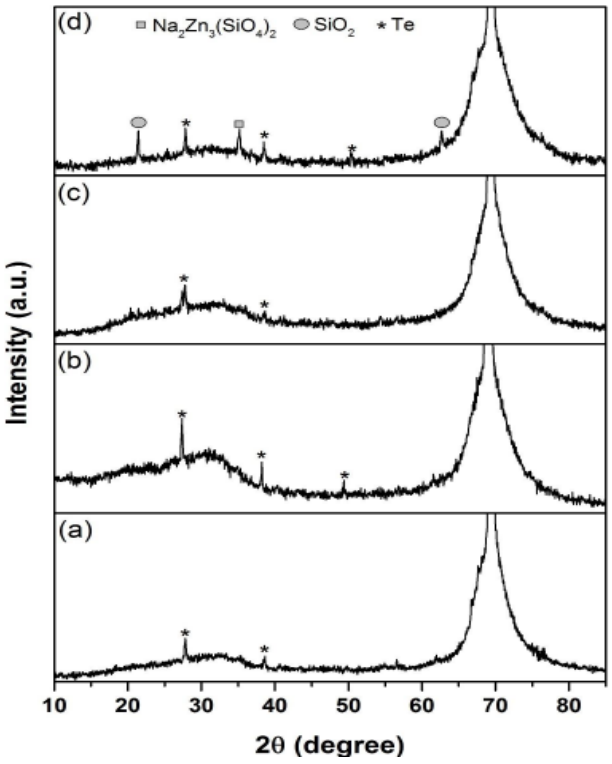

Fig. 4. XRD patterns of doped layer on Si_3N_4-on-silicon fabricated under (a) vacuum (SV), (b) oxygen (SO), (c) nitrogen (SN) and (d) argon (SA) environment.

Figure 5 presents the Raman spectra for the samples doped under a vacuum and with various types of the background gas. All the spectra exhibited a similar pattern, except the intensity of the Si peak (521 cm^{-1}), which depended on the thickness of the doped layer. The Si peak that is associated with the silicon substrate is more pronounced for the thinner film. The peaks at 122 and 141 cm^{-1} are attributed with metallic tellurium. The Raman peak at 272 cm^{-1} is assigned to a TeO_3 trigonal pyramid (tp) bending vibration [19,20] while peak in the ranged of 430-490 cm^{-1}, is often attributed to Q4 species of Si-O-Si bending [21,22]. The emergence peak at approximately 590-640 cm^{-1} is corresponded to the bending vibration of Si-O-Si between two Q2 species [23,24]. The presence of Raman peak in the region around 770-800 cm^{-1} are commonly associated with antisymmetric Si vibration in tetrahedral oxygen cage (Q4) [21,23] while peak in the 900-1000 cm^{-1} range is usually corresponded to Si-O-Si stretching of Q2 components [24,25]. For peaks located at a high wavenumber, 1160 and 1544 cm^{-1}, these two peaks are linked with erbium fluorescence emission [26].

The PL spectra for samples SV, SO, SN and SA are shown in Figure 6. The PL intensity for each sample corresponds to the amount of Er^{3+} ions embedded in the doped layer. Based on the PL spectra obtained, it showed that the SO sample had the highest amount of Er^{3+} followed by SN, SA and SV. The sample fabricated in a vacuum atmosphere (SV) experienced re-sputtering incidents,

causing a reduction of Er^{3+} ions in the doped layer. However, all samples exhibited silicate-based characteristics according to the FWHM and PL lifetime [27,28], as listed in Table 3. This indicates that the Er-TZN had indeed modified the Si_3N_4 network and formed silicate glass, by considering nitrogen gas in Si_3N_4 was lost in the form of N_2 gas when TeO_2 plasma plume react with Si_3N_4 [2]. It also shows the PL lifetime had an inverse relationship with PL intensity. The decline in the PL lifetime due to the higher Er^{3+} ion concentration in the doped layer that decrease the average spacing between Er-Er ions and this cause the quenching effect because of energy migration between Er^{3+} ions.

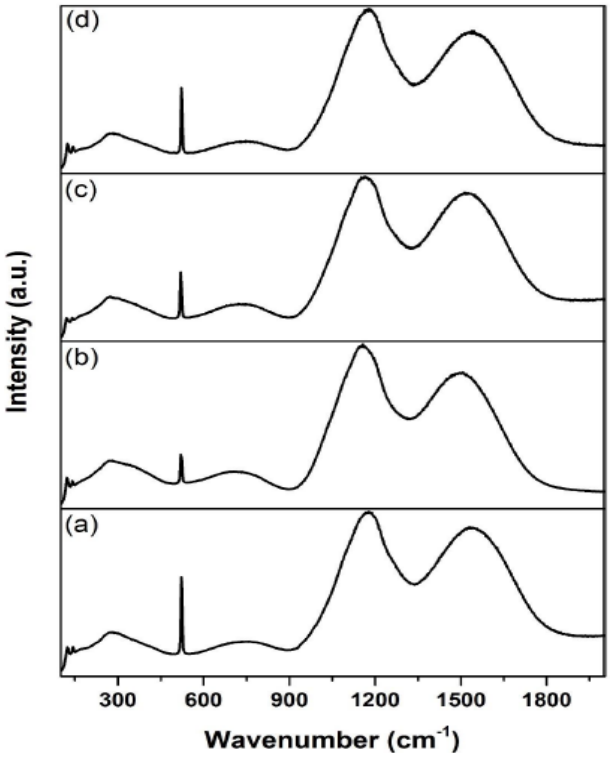

Fig. 5. Raman spectra for samples doped under (a) vacuum (SV), (b) oxygen (SO), (c) nitrogen (SN) and (d) argon (SA) environment.

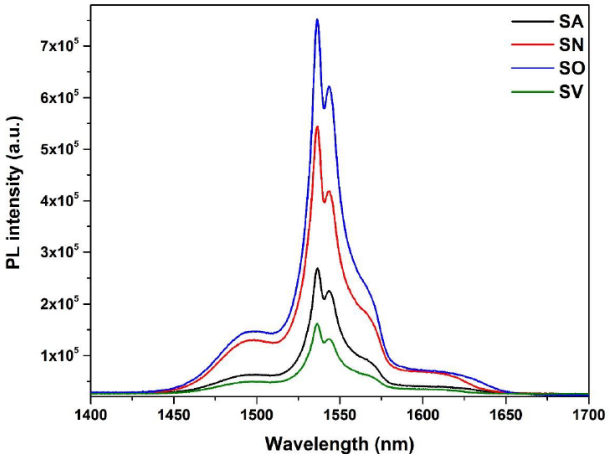

Fig. 6. PL spectra for samples SV, SO, SN and SA.

Table 3. PL lifetime and FWHM for doped layer prepared under different atmospheres.

Samples	PL lifetime (ms)	FWHM (nm)
SV	10.55	20
SO	8.45	20
SN	8.89	20
SA	10.43	20

4. Conclusion

In summary, the thickness of the doped layer depends on the ambient atmosphere in the chamber during ULPD process. Doped layer under vacuum is the thinnest among all of the samples. The very high kinetic energy of a particle in the plasma plume can be reduced by deliberately introducing a background gas in the chamber at low pressures. A homogeneous layer failed to be obtained due to a high melting temperature (1900 °C) and rigid structure of Si_3N_4. XRD patterns showed that all samples are is in a mixed amorphous-crystalline phase. All Raman spectra exhibited a similar pattern, except the intensity of the Si peak (521 cm^{-1}), which depended on the thickness of the doped layer. All samples exhibited silicate-based characteristics according to the FWHM and PL lifetime, indicating the Er-TZN had indeed modified the Si_3N_4 network and formed silicate glass, by considering nitrogen gas in Si_3N_4 was lost in the form of N_2 gas when TeO_2 plasma plume react with Si_3N_4

Acknowledgements

Authors would like to acknowledge the funding from the Engineering and Physical Sciences Research Council (EPSRC)(EP/M015165/1).

References

[1] Kamil S A, Chandrappan J, Krauss T F, Jose G, J. Optoelectron. Adv. M. **21**(11-12), 710 (2019).

[2] Kamil S A and Jose G 2020 Nanomaterials. 12 919; https://doi.org/10.3390/nano12060919

[3] Chandrappan J, Murray M, Petrik P, Agocs E, Zolnai Z, Tempez A et al 2015 Opt. Mater. Express. 5 2849; https://doi.org/10.1364/OME.5.002849

[4] Chandrappan J, Murray M, Kakkar T, Petrik P, Agocs E and Zolnai Z 2015 Sci. Rep. 5 14037; https://doi.org/10.1038/srep14037

[5] Kamil S A, Chandrappan J, Portoles J, Steenson P and Jose G 2019 Mater. Res. Express. 6 086220; https://doi.org/10.1088/2053-1591/ab28eb

[6] Kamil S A, Chandrappan J, Murray M, Steenson P, Krauss T F and Jose G 2016 Opt. Lett. 41 4684; https://doi.org/10.1364/OL.41.004684

[7] Gamaly E G, Rode A V, Luther-Davies B and Tikhonchuk V T 2002 Phys. Plasmas. 9 949; https://doi.org/10.1063/1.1447555

[8] Dlamini S T S, Swart H C, Terblans J J and Ntwaeaborwa O M 2013 Solid State Sci. 23 65; https://doi.org/10.1016/j.solidstatesciences.2013.06.009

[9] Marozau I, Shkabko A, Döbeli M, Lippert T, Logvinovich D and Mallepell M et al 2009 Materials 2 1388; https://doi.org/10.3390/ma2031388

[10] Kek R, Yap S L, Koh S F, Nee C H, Tou T Y and Yap S S 2020 Thin Solid Films 701 137953; https://doi.org/10.1016/j.tsf.2020.137953

[11] Boffoué M O, Lenoir B, Scherrer H and Dauscher A 1998 Thin Solid Films 322 132; https://doi.org/10.1016/S0040-6090(97)00912-7

[12] Hasabeldaim E, Ntwaeaborwa O M, Kroon R E, Motaung D E, Coetsee E and Swart H C 2017 Opt. Mater. 74 76; https://doi.org/10.1016/j.optmat.2017.04.061

[13] Ojeda G P A, Schneider C W, Döbeli M, Lippert T and Wokaun A 2017 J. Appl. Phys. 121 135306; https://doi.org/10.1063/1.4979780
[14] Chen X, Xiong S, Sha Z and Liu Z 1997 Appl. Surf. Sci. 115 279; https://doi.org/10.1016/S0169-4332(96)01087-2
[15] Haile H T and Dejene F B 2020 Mater. Res. Express 7 076406; https://doi.org/10.1088/2053-1591/ab88fd
[16] Chen T, Li X M, Zhang S and Zeng H R 2004 J. Cryst. Growth. 270 553; https://doi.org/10.1016/j.jcrysgro.2004.07.021
[17] Coetsee E, Terblans J J and Swart H C 2009 Phys. B 404 4431; https://doi.org/10.1016/j.physb.2009.09.046
[18] Martín-Sánchez J, Chahboun A, Pinto S R C, Rolo A G, Marques L, Serna R et al 2013 Appl. Phys. A Mater. Sci. Process 110 585; https://doi.org/10.1007/s00339-012-7131-z
[19] Ghoshal S K, Awang A, Sahar M.R and Arifin R 2015 J. Lumin. 159 265; https://doi.org/10.1016/j.jlumin.2014.11.032
[20] Dousti M R, Sahar M R, Amjad R J, Ghoshal S K and Awang A 2013 J. Lumin. 143 368; https://doi.org/10.1016/j.jlumin.2013.04.017
[21] Seuthe T, Grehn M, Mermillod-Blondin A, Eichler H J, Bonse J and Eberstein M 2013 Opt. Mater. Express. 3 755; https://doi.org/10.1364/OME.3.000755
[22] Suresh B, Zhydachevskii Y, Brik M G, Suchocki A and Reddy M S 2016 J. Alloys Compd. 683 114; https://doi.org/10.1016/j.jallcom.2016.05.056
[23] Bourhis K, Shpotyuk Y, Massera J, Aallos V, Jouan T, Boussard-plédel C et al 2014 Opt. Mater. 37 87; https://doi.org/10.1016/j.optmat.2014.05.004
[24] Robinet L, Coupry C, Eremin K and Hall C 2006 J. Raman Spectrosc. 37 787 https://doi.org/10.1002/jrs.1549
[25] McMillan P 1984 Am. Mineral. 69 622
[26] Cui J and Hope G A 2015 J. Spectrosc. 2015 940172
[27] Polman A 1997 Appl. Phys. Rev. 82 1; https://doi.org/10.1063/1.366265
[28] Snoeks E, Kik P G and Polman A 1996 Opt. Mater. 5 159; https://doi.org/10.1016/0925-3467(95)00063-1